Heterogeneous & Homogeneous & Bio-
CHEMCATCHEM
CATALYSIS

Supporting Information

Molybdenum Sulfides and Selenides as Possible Electrocatalysts for CO_2 Reduction

Karen Chan,[a] Charlie Tsai,[a] Heine A. Hansen,[a] and Jens K. Nørskov*[a, b]

cctc_201402128_sm_miscellaneous_information.pdf

Calculation Details

For non-adsorbed species, electronic energies were converted to chemical potentials at 298.15K using standard ideal-gas methods[1]. Free energy corrections for these species, which include zero point energies, heat capacities, and entropies, are shown in Table S 1. All gaseous species from CO_2 reduction were assumed to have a fugacity of 101325 Pa. The free energy of liquid water was calculated as an ideal gas, and adjusted to a fugacity of 3534 Pa, the vapor pressure of water at room temperature. The free energy of CH_3OH and HCOOH were adjusted to fugacities of 6080 and 19 Pa, respectively, to give an aqueous activity of 0.01[2]. For H_2S, COS, and COSe, we assumed pressures of 1.01 Pa; in the case of H_2S, this corresponds to an aqueous activity of $1x10^{-6}$ M, a standard concentration for corrosion resistance[3].

With the RPBE functional[4], molecules with an OCO or OCS backbone are poorly described; a sensitivity analysis based on experimentally determined gas-phase reaction energies gave a systematic correction of +0.45eV[5,2,6]. Similarly, a sensitivity analysis of the BEEF-vdW functional found that, while most of the error still resides in OCO, a +0.33eV correction for OCO, plus +0.09eV for H_2 led to a slightly larger improvement in the energetics of gas-phase species[7]. We have applied these corrections in this work.

Molecule	Fugacity (Pa)	*ZPE* (eV)	$\int C_p \, dT$ (eV)	$-TS$ (eV)
CO_2	101325	0.31	0.10	-0.66
CO	101325	0.13	0.09	-0.61
H_2	101325	0.28	0.09	-0.40
H_2O	3534	0.57	0.10	-0.67
CH_3OH	6080	1.37	0.12	-0.81
HCOOH	19	0.90	0.11	-0.99
CH_4	101325	1.20	0.11	-0.58
CH_2O	101325	0.71	0.11	-0.68
H_2S	1.01	0.40	0.10	-0.93
COS	1.01	0.25	0.10	-1.01
COSe	1.01	0.22	0.11	-1.05

Table S 1 Free energy corrections for non-adsorbed species .

Adsorbate binding and free energies were calculated with the lowest energy adsorbate configuration. The binding energies of CO, COOH, CHO are, respectively,

$$E_b(CO) = E(*CO) + \Delta E_{sol}(CO) - E* - E(CO_{(g)})$$
$$E_b(COOH) = E(*COOH) + \Delta E_{sol}(COOH) - E* - E(CO_{2(g)}) - 1/2E(H_2)$$
$$E_b(CHO) = E(*CHO) + \Delta E_{sol}(CHO) - E* - E(CO_{(g)}) - 1/2E(H_2)$$

Where ΔE_{sol} indicates a solvation correction to the calculated adsorbate energy; $\Delta E_{sol}(COOH) = -0.25eV$, and $\Delta E_{sol}(CHO) = \Delta E_{sol}(CO) = -0.1eV$[5].

Free energies G of adsorbate states are calculated by adding the zero-point energies, entropies, and heat capacities, calculated with the harmonic oscillator approximation where all degrees of freedom of the adsorbates were treated as harmonic vibrations[1]. Table S 2 lists these free energy corrections applied. As in the binding energy calculations, we have approximated the effect of solvation using previously determined corrections[5]: -0.5eV for *OH, -0.25eV for *R-OH (i.e. a hydroxyl indirectly bound via other atoms), and -0.1eV for *CO and *CHO.

Adsorbate	*ZPE* (eV)	$\int C_p \, dT$ (eV)	*-TS* (eV)
*C	0.09	0.23	-0.04
*CH	0.34	0.03	-0.05
*CO	0.19	0.08	-0.16
*OH	0.36	0.05	-0.08
*CHOH	0.81	0.07	-0.13
*OCHO	0.62	0.11	-0.24
*O	0.07	0.03	-0.04
*CHO	0.45	0.09	-0.18
*OCH_3	1.11	0.10	-0.19
*CH_2	0.61	0.05	-0.09
*CH_3	0.93	0.07	-0.13
*CH_2OH	1.07	0.10	-0.22
*COH	0.48	0.08	-0.14
*COOH	0.62	0.10	-0.19
*H	0.23	0.01	-0.01
*S	0.06	0.03	-0.05
*SH	0.27	0.06	-0.11
*Se	0.04	0.05	-0.09
*SeH	0.22	0.069	-0.14

Table S 2 Free energy corrections for adsorbed species.

Coverage determination

At $U > 0V_{RHE}$, where hydrogen evolution does not occur, the edge configurations can be determined by thermodynamics. We minimize the edge free energy γ [8,9]:

$$\gamma = \frac{1}{2L}\left[G_{stripe} - N_M E^{bulk}_{MoS_2} - \left(2N_{Mo} - N_S\right)\mu_S - N_H \mu_H \right]$$

where G_{stripe} is the stripe free energy, $E^{bulk}_{MoS_2}$ the bulk energy of MoS_2, and μ_i the chemical potential of the i^{th} species. As we apply an infinite stripe model, γ is the average edge energy of both the Mo and S edges; however, the relative stability of various coverages on either the Mo or S edge can be determined by comparing the γ of stripes with the other edge in the same configuration. The relative stability of Mo or S/Se edges are determined by their absolute edge energies, which can be calculated via cluster

calculations[10]. Under the reducing conditions of interest, previous cluster calculations on MoS_2 suggest the Mo edge to be more stable than the S, with their predominance determined by a Wulff construction[11].

The chemical potentials of sulfur and hydrogen are determined by the following equilibria,

$$S + 2H^+ + 2e^- \rightleftharpoons H_2S$$

$$H \rightleftharpoons H^+ + e^-.$$

Again, we apply the computational hydrogen electrode model[12], where the chemical potential of a proton-electron pair is $\mu(H^+) + \mu(e^-) = \frac{1}{2}\mu(H_2) - eU$, where U is defined relative to RHE. Therefore,

$$\mu(S) = \mu(H_2S) - 2\left(\frac{1}{2}\mu(H_2) - eU\right)$$

$$\mu(H) = \frac{1}{2}\mu(H_2) - eU\,.$$

$\mu(H_2S)$ is determined by assuming a pressure $P(H_2S)$ = 10^{-5}-10^{-8} bar (~10^{-6} – 10^{-9} M) corresponding to a standard corrosion resistance[3].

At $U < 0V_{RHE}$, the coverage is determined by kinetics. As discussed in the main text, activation energies of surface reactions, in general, scale with reaction energies; we therefore make kinetic arguments based on thermodynamic reaction energies. We assume that, starting with the thermodynamically stable coverage at $0V_{RHE}$, the steady state hydrogen coverage is where H_2 evolution is more downhill than further H adsorption or H_2S evolution. Figure S 1 to S 6 illustrate the free energy diagrams for these proton transfer steps for all edges; generally, we identify the stable coverage to be the state of lowest free energy in the last proton transfer step shown.

For the Mo edge of $MoSe_2$, both θ_S=0.5 and θ_S=0.75, θ_H=0.125 are stable within the range of considered $P(H_2S)$, so we consider both coverages in the present work. In the case of the S edge of MoS_2, illustrated in Figure S 2, there is only a <0.1eV difference between H adsorption or H_2 evolution in the first proton transfer step shown. This difference is around the accuracy of DFT calculations as well as the +0.09eV correction applied to the electronic energy of H_2. The steady state coverage may therefore lie between 3H* or 4H* (θ_H=0.375 or 0.5), which can only be studied by larger model system sizes. We consider the CO_2 reduction activity for both θ_H=0.375 and 0.5 in the present work.

In principle, the same argument can be made for the Mo edge of $MoSe_2$ at θ_S=0.75, where there is also a small difference between H adsorption or H_2 evolution in the first proton transfer step shown. Given the accuracy of our calculations, the stable θ_H may lie between 0 or 0.125. However, since E_b(COOH) and E_b(CHO) for these two coverages also differ by only <0.15eV (See Figure S 7 and S 8), and neither coverage is expected to bind CO, we consider only the θ_H=0.125 coverage further.

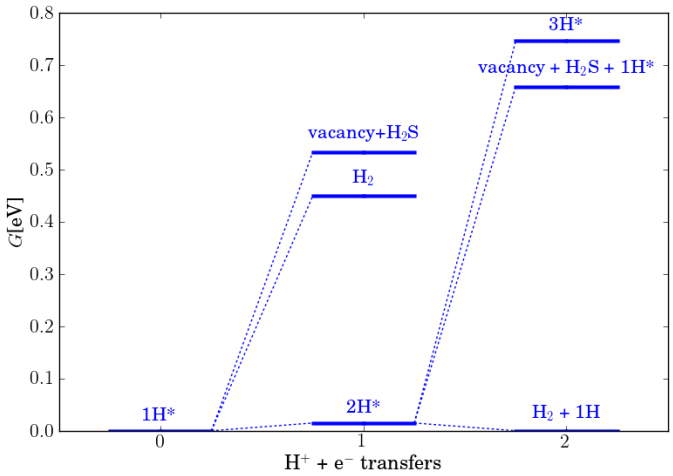

Figure S 1. Free energy diagram for hydrogen adsorption, H_2 and H_2S evolution on the Mo edge of MoS_2, θ_s=0.5

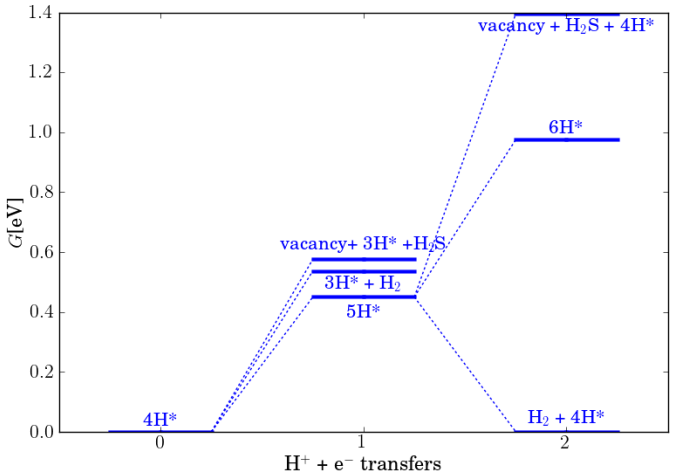

Figure S 2. Free energy diagram for hydrogen adsorption, H_2 and H_2S evolution on the S edge of MoS_2, θ_s=1

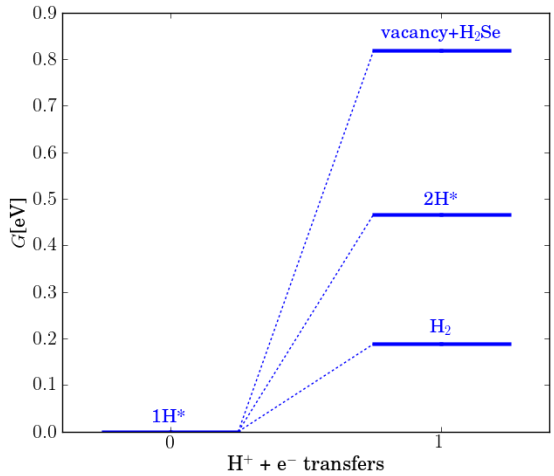

Figure S 3. Free energy diagram for hydrogen adsorption, H_2 and H_2Se evolution on the Mo edge $MoSe_2$, θ_{Se}=0.5

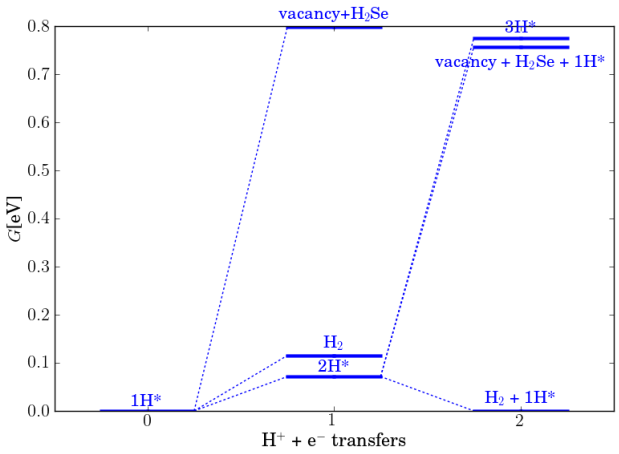

Figure S 4. Free energy diagram for hydrogen adsorption, H_2 and H_2Se evolution on the Mo edge $MoSe_2$, θ_{Se}=0.75

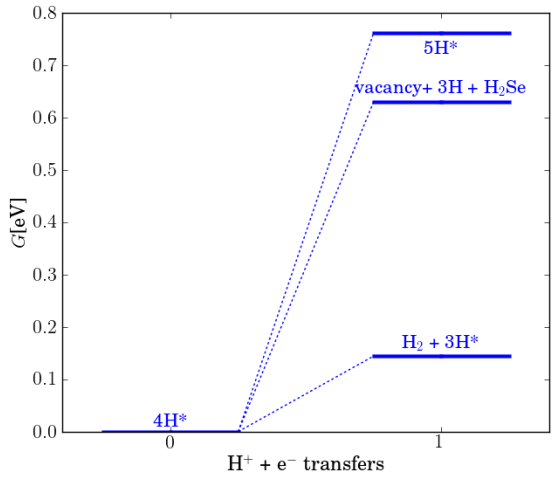

Figure S 5. Free energy diagram for hydrogen adsorption, H_2 and H_2Se evolution on the Se edge $MoSe_2$, θ_{Se}=1

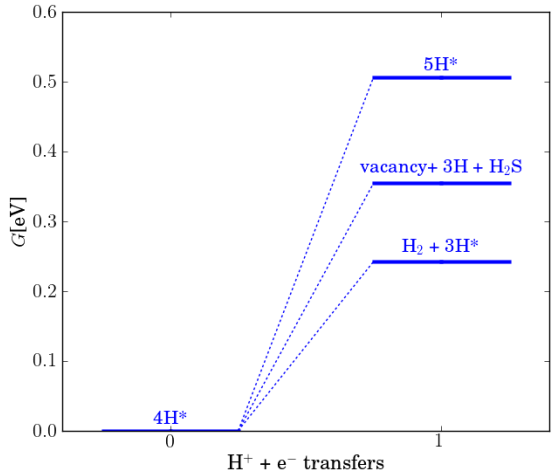

Figure S 6. Free energy diagram for hydrogen adsorption, H_2 and H_2Se evolution on the Ni doped S edge MoS_2, θ_S=0.5

Scaling of E_b(COOH) and E_b(CHO) vs. E_b(CO) – coverage dependence

In principle, θ_S and θ_H would only be rigorously determined via a full kinetic model, which is beyond the scope of this work. In Figure S 7 and S 8, we show the scaling relations of E_b(COOH) and E_b(CHO) vs. E_b(CO) at a variety of edge coverages. In many cases, slight variations in coverages from those assumed still lead to a substantial destabilization of COOH and CHO relative to the transition metal scaling line.

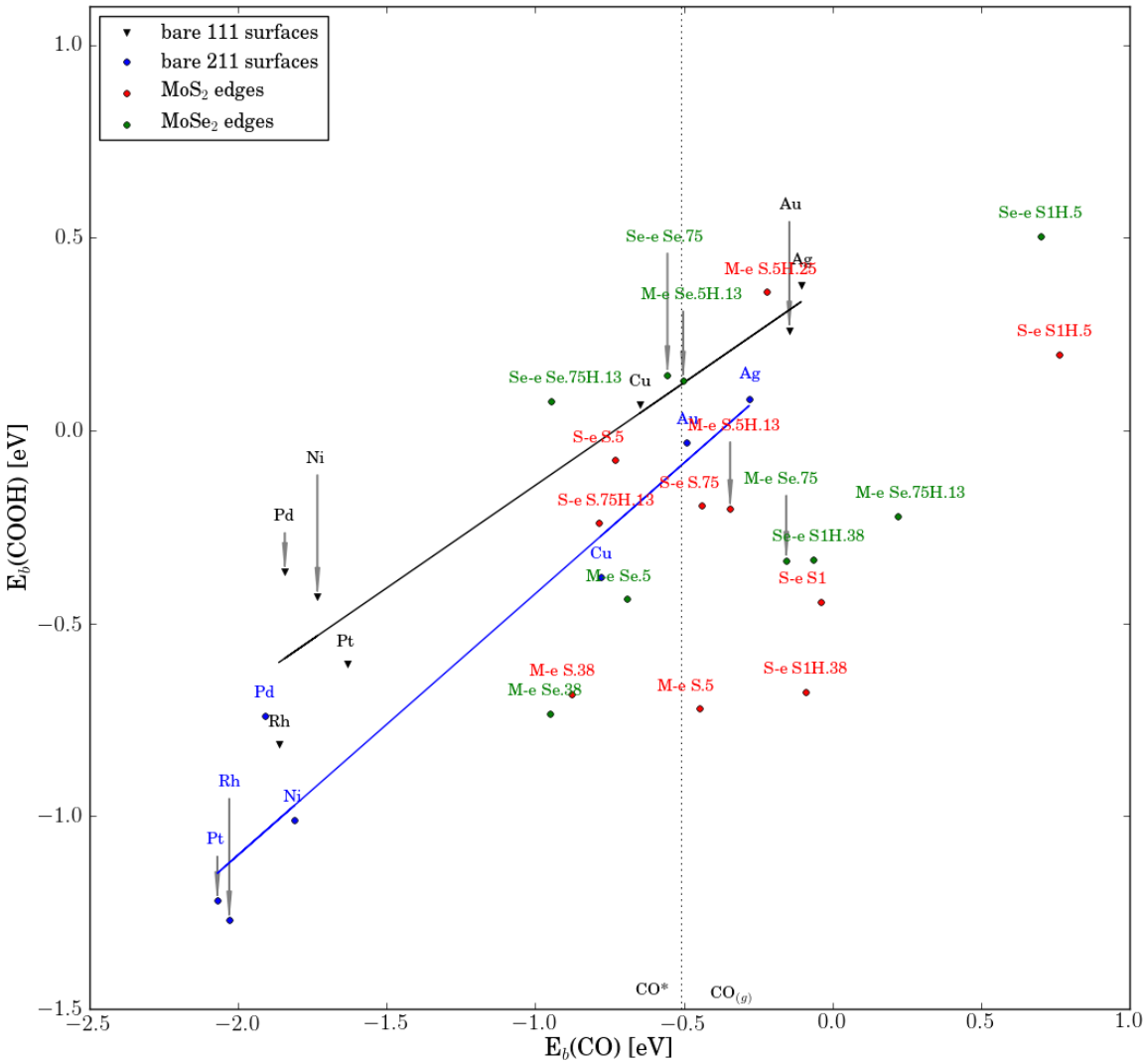

Figure S 7. Scaling relations for E_b(COOH) vs. E_b(CO) at various θ_S and θ_H. Mo edges are denoted M-e, S by S-e; coverages of S and H are indicated by S and H in the data label, i.e. S1H.38 indicates θ_S = 1 and θ_H=0.38. Bare transition metal 111 and 211 scaling lines, determined using the RPBE functional, are also shown for comparison[5,13].

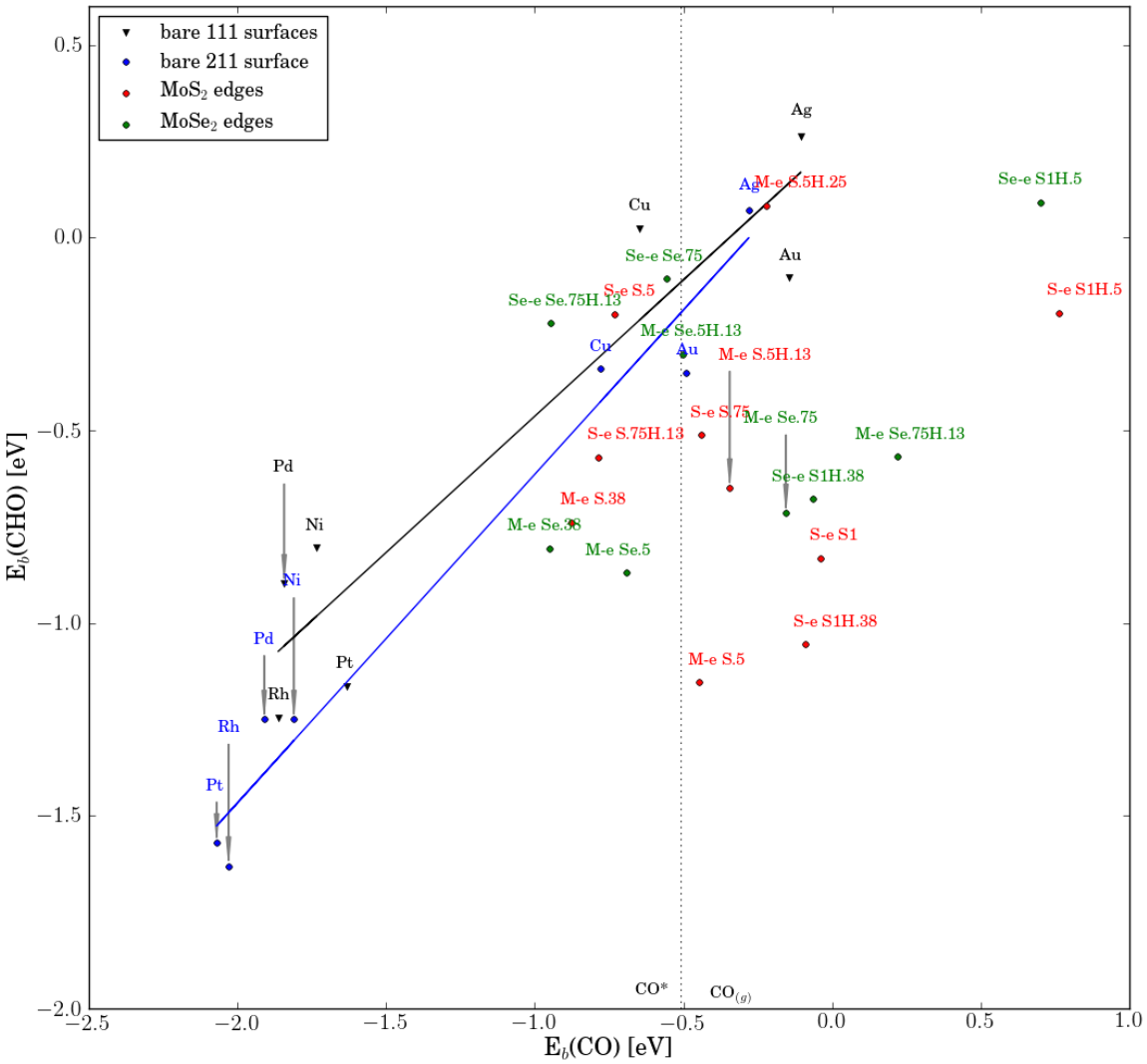

Figure S 8. Scaling relations for E_b(CHO) vs. E_b(CO) at various θ_S and θ_H. Mo edges are denoted M-e, S by S-e; coverages of S and H are indicated by S and H in the data label, i.e. S1H.38 indicates θ_S = 1 and θ_H=0.38. Bare transition metal 111 and 211 scaling lines, determined using the RPBE functional, are also shown for comparison[5,13].

Reaction paths for bare Cu(211), Au(211)

For comparison, we show the lowest free energy pathway for CO_2 reduction on bare Cu(211) and Au(211) surfaces in Figure S 9, taken from Refs. [2,5].

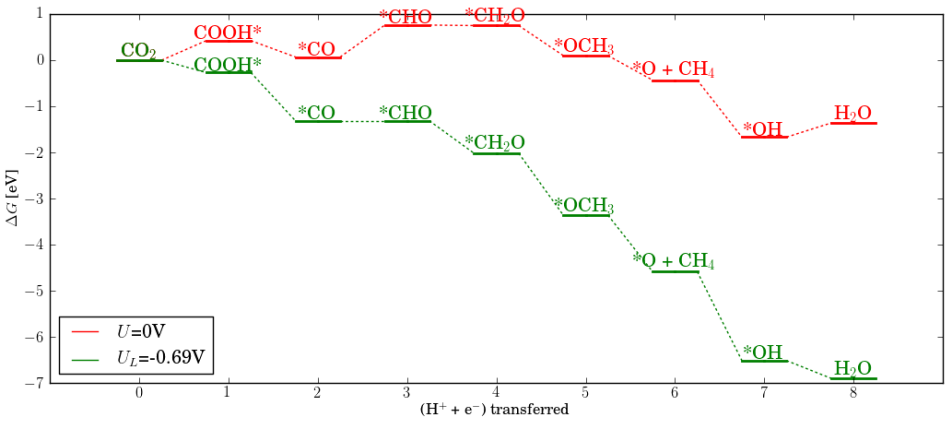

(a)

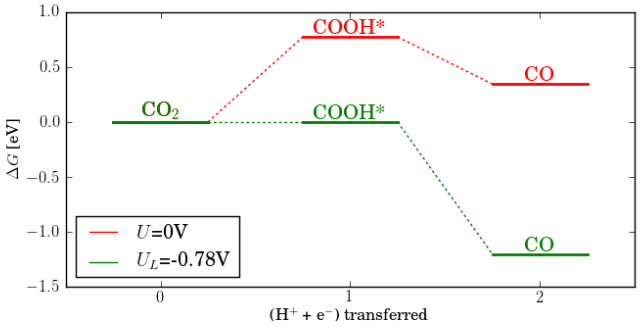

(b)

Figure S 9 Lowest free energy paths for CO_2 reduction on Cu(211) (a) and Au(211) (b), at both U=0V and U_L. Data from Ref. [2,5].

Alternate Reaction Paths

Figure S 10 to Figure S 16 show the free energies of alternate reaction paths for the edges considered, at U=0V vs. RHE. In all cases, COOH binds more strongly than formate (OCHO), suggesting that formic acid (HCOOH) formation is not favored. In the case of the Mo edge of $MoSe_2$ at $\theta_{Se} = 0.5$ and the Ni-doped S edge of MoS_2, methanol (CH_3OH) formation is also possible; however, it was previously determined that barriers for proton transfers to C sites are much higher than proton transfers to O, which could result in a higher selectivity towards CH_4 [13].

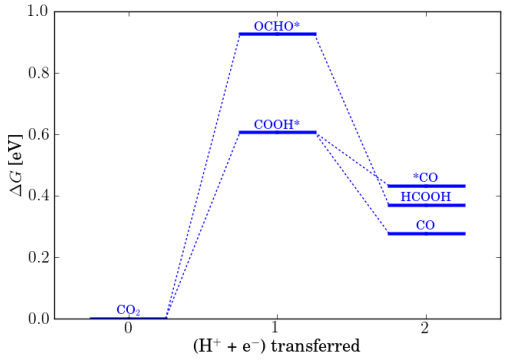

Figure S 10. Free energy diagram of CO_2 reduction to CO on Mo edge of MoS_2

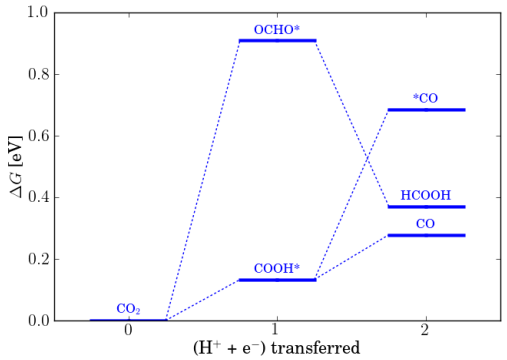

Figure S 11. Free energy diagram of CO_2 reduction to CO on S edge of MoS_2 with $\theta_H = 0.375$

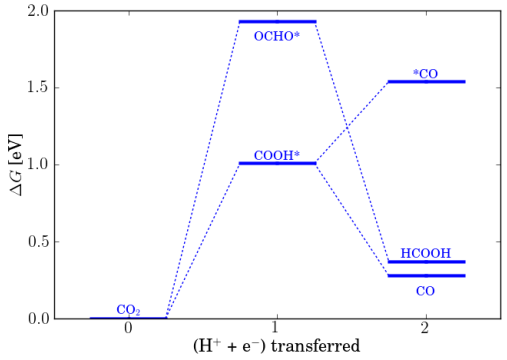

Figure S 12. Free energy diagram of CO_2 reduction to CO on S edge of MoS_2 with $\theta_H = 0.5$

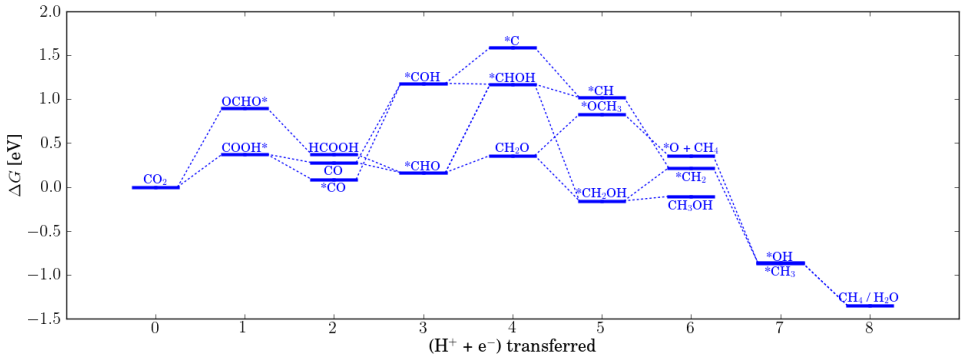

Figure S 13 Free energy diagram of CO_2 reduction to CH_4 and CH_3 on the Mo edge of $MoSe_2$, θ_s =0.5

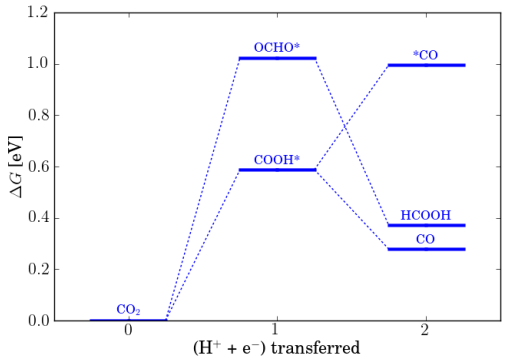

Figure S 14 Free energy diagram of CO_2 reduction to CO on the Mo edge of $MoSe_2$, $\theta_s = 0.75$, θ_H =0.125

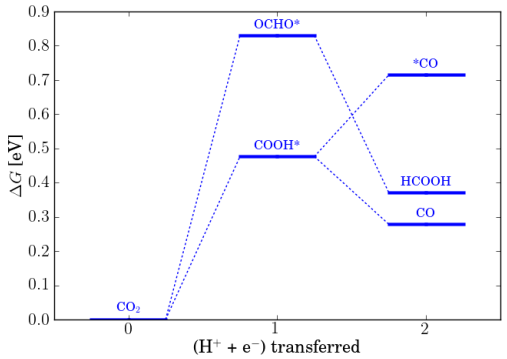

Figure S 15 Free energy diagram of CO_2 reduction to CO on the Se edge of $MoSe_2$

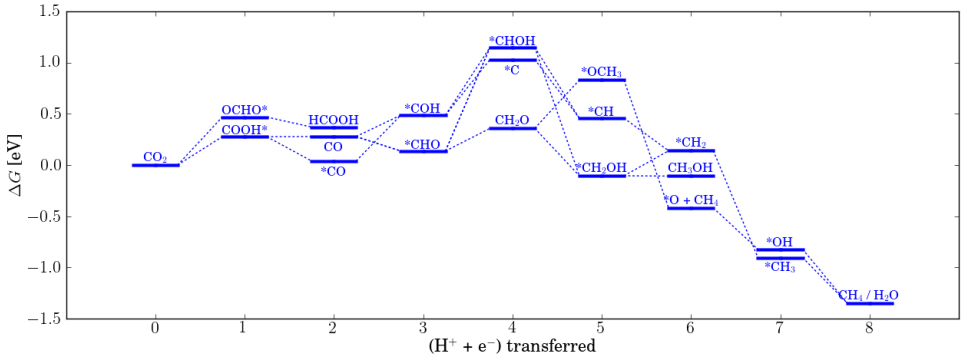

Figure S 16 Free energy diagram of CO_2 reduction to CH_4 and CH_3 on the Ni doped S edge of MoS2

COS/COSe formation

We also considered the relative stability of the edges against COS/COSe formation[6]. Figure S 17 shows the free energy diagrams for COS/COSe formation for all edges. The S edge of MoS_2 (θ_H = 0.375) and Ni-doped MoS_2 are less stable than other edges, and a change in the P(COS)/P(COSe) assumed does not affect this trend. Ultimately, kinetics determine the dissolution rate. Both MoS_2 and $MoSe_2$ have been shown to retain their hydrogen evolution activity under repeated cycling (1000 cycles) down to -0.4 and -0.45V_{RHE}, respectively[14], [15].

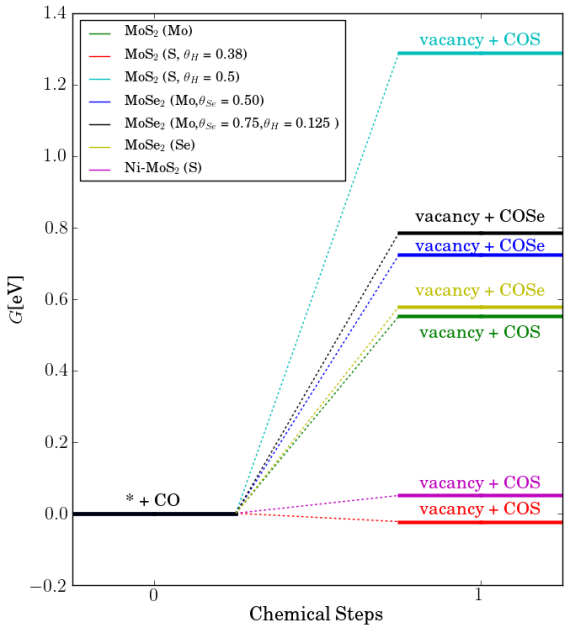

Figure S 17 Free energy diagram for COS/COSe formation from stable Mo/S/Se edge configurations

1. Cramer, C. J. (2013). *Essentials of Computational Chemistry: Theories and Models* , .

2. Peterson, A. A., Abild-Pedersen, F., Studt, F., Rossmeisl, J., & Norskov, J. K. (2010). *Energy Environ. Sci.* 3, 1311-1315.

3. Pourbaix, M. (1974). *Atlas of electrochemical equilibria in aqueous solutions* , .

4. Hammer, B., Hansen, L. B., & Nørskov, J. K. (1999). *Physical Review B* 59, 7413.

5. Peterson, A. A. & Nørskov, J. K. (2012). *The Journal of Physical Chemistry Letters* 3, 251--258.

6. Varley, J. B., Hansen, H. A., Ammitzbøll, N. L., Grabow, L. C., Peterson, A. A., Rossmeisl, J., & Nørskov, J. K. (2013). *ACS Catalysis* 3, 2640-2643.

7. Studt, F., Abild-Pedersen, F., Varley, J. B., & Nørskov, J. K. (2013). *Catalysis letters* 143, 71--73.

8. Raybaud, P., Hafner, J., Kresse, G., Kasztelan, S., & Toulhoat, H. (2000). *Journal of Catalysis* 189, 129--146.

9. Bollinger, M., Jacobsen, K. W., & Nørskov, J. K. (2003). *Physical Review B* 67, 085410.

10. Schweiger, H., Raybaud, P., & Toulhoat, H. (2002). *Journal of Catalysis* 212, 33--38.

11. Schweiger, H., Raybaud, P., Kresse, G., & Toulhoat, H. (2002). *Journal of Catalysis* 207, 76--87.

12. Nørskov, J. K., Rossmeisl, J., Logadottir, A., Lindqvist, L., Kitchin, J. R., Bligaard, T., & Jonsson, H. (2004). *The Journal of Physical Chemistry B* 108, 17886--17892.

13. Shi, C., Hansen, H. A., Lausche, A. C., & Norskov, J. K. (2014). *Phys. Chem. Chem. Phys.* , -.

14. Li, Y., Wang, H., Xie, L., Liang, Y., Hong, G., & Dai, H. (2011). *Journal of the American Chemical Society* 133, 7296--7299.

15. Kong, D., Wang, H., Cha, J. J., Pasta, M., Koski, K. J., Yao, J., & Cui, Y. (2013). *Nano letters* 13, 1341--1347.